Transparent and Colorless Dye-Sensitized Solar Cells Based on Pyrrolopyrrole Cyanine Sensitizers

Thibaut Baron, Waad Naim, Ilias Nikolinakos, Yann Pellegrin, Denis Jacquemin, Stefan Haacke, Frédéric Sauvage, Fabrice Odobel

RESEARCH ARTICLE

Transparent and Colorless Dye-Sensitized Solar Cells Based on Pyrrolopyrrole Cyanine Sensitizers

Thibaut Baron,[a#] Waad Naim,[b#] Ilias Nikolinakos,[c#] Baptiste Andrin,[a] Yann Pellegrin,[a] Denis Jacquemin,[*a] Stefan Haacke,[*c] Frédéric Sauvage,[*b] and Fabrice Odobel[*a]

[#]these authors equally contributed to this study

[a] Dr. T. Baron, Mr. Baptiste Andrin, Dr. Y. Pellegrin, Dr. D. Jacquemin, Dr. F. Odobel
Nantes Université, CNRS, CEISAM, UMR-6230, F-44000, Nantes, France E-mail: Fabrice.Odobel@univ-nantes.fr and denis.jacquemin@univ-nantes.fr
[b] Dr. W. Naim, Dr. F. Sauvage
LRCS, CNRS UMR 7314, 80039 Amiens
Université de Picardie Jules Verne (UPJV)
15 Rue Baudelocque, 80000 Amiens, France E-mail: frederic.sauvage@u-picardie.fr
[c] I. Nikolinakos, Dr. S. Haacke
IPCMS, CNRS UMR 7504
Université de Strasbourg
23 Rue du Loess Bâtiment 69, 67200 Strasbourg, France E-mail: stefan.haacke@ipcms.unistra.fr

Supporting information for this article is given via a link at the end of the document.

Abstract: The development of transparent solar cells extends the applications of photovoltaics by offering the opportunity to substitute the gigantic surface coverage of windows by solar panels to produce electricity. In this contribution, we report a new family of NIR-sensitizers based on pyrrolopyrrole cyanine dyes, particularly efficient for the development of fully transparent and colorless dye sensitized solar cells since a record efficiency of 2.5% was achieved with an average visible transmittance (AVT) of 76% and a color rending index (CRI) of 93.

Introduction

The increasing global energy consumption demands a greater variety of clean and sustainable power sources. In this context, photovoltaics (PV) is undoubtedly an attractive and most relevant response to this challenge as solar energy can meet our ever increasing global energy needs. Today, silicon-based solar modules account for more than 90% of the current PV installations, and several tenths of GW of electricity are currently produced with this technology. Transparent photovoltaics (TPV) is a disruptive and emerging technology in which the solar cells selectively transmit the visible light to human eyes but harvest UV and/or NIR photons.[1] TPV is attractive as it widens the deployment of PV into new sectors, where opaque panels such as silicon are unsuitable. For example, TPV can enter the market of building integrated photovoltaics (BIPV) with power-generating solar facades and can also equip greenhouses, car windows, and sunglasses, providing thus an immense potential to generate solar electricity beyond the conventional rooftops and solar power plants.[1–3] Additionally, when NIR solar irradiation generates electricity, it improves the energy saving of the buildings and provides heat insulation functionality. There are two main approaches to TPV.[4] The first one relies on non-wavelength-selective absorbing materials, whose transparency is provided either by laser patterning segmented cells or thinning the absorbing layer until semi-transparency is reached. The second category is based on wavelength-selective absorbers, and that can reach a maximum theoretical efficiency of 20.6% with 100% average visible transmittance (AVT), while the PCE of non-wavelength- selective TPV approaches 0% as the AVT is over 90%.[5] The typical best performing non-wavelength-selective TPV cells are based on perovskite solar cells that display power conversion efficiency (PCE) of 7.5-12% with AVT between 20-52% while organic solar cells demonstrate the best wavelength-selective PCEs situated respectively between 4% and 10% for AVTs between 40% and 60% and light utilization efficiency of 2.2–3.7%.[2] These considerations tend to support that TPV will be most likely dominated by molecular absorbers as their discrete absorption bands allow for more selective light harvesting. In this regard, dye sensitized solar cells (DSSCs) are particularly attractive as they present unique features such as transparency for both sides, which allows intrinsically see-through devices, color tunability with the choice of the dye providing high aesthetic property and finally stability as proven by ageing tests.[6] Among the myriad of dyes developed and tested for DSSCs, the vast majority exploits visible photons only (until 700 nm).[5] So far, there are only few examples of dyes with significant incident photon to current efficiency (IPCE) extending in the near infrared (NIR) region such as ruthenium,[7,8] osmium complexes[9] and some organic sensitizers.[10,11] Among them even fewer selectively harvest only the NIR region and remain transparent in the visible range. Notable examples are the squaraine dye (coded HSQ5) developed by Han and co-workers[12] with a 3.66% PCE and transmittance of 60% at 560 nm and very recently reported by Sauvage and co-workers,[13] the cyanine dye (coded VG20) which exhibits a PCE of 3.10% with an impressive AVT of 76%. Pyrrolopyrrole cyanine dyes is a class of near-infrared dyes and fluorophores first reported by Daltrozzo and co-workers,[14] that has been mainly used for biological applications such as imaging and photoacoustic applications.[15–18] As cyanine dyes, pyrrolopyrrole cyanines (PPcys) display intense and narrow absorption bands located in the low energy part of the spectrum (between 700-800 nm depending on the substituents) and they exhibit usually high fluorescence quantum

yields (around 0.4-0.6).[19] As such, they fulfill some of the key criteria to develop NIR sensitizers for TPV, prompting us to explore for the first time their potential for see-through and transparent DSSCs. Here, we report two blatantly transparent pyrrolopyrrole cyanine dyes **TB144** and **TB207** that selectively harvest NIR photons with unprecedented power conversion efficiency (4%) as regards to their transparency (AVT =76% with corresponding PCE of 2.5%) (Figure 1).

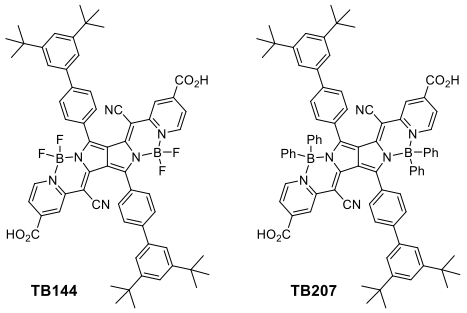

Figure 1. Structure of the dyes **TB144** and **TB207**.

The synthesis of the dyes **TB144** and **TB207** requires the soluble diketopyrrolopyrrole **7** starting reagent and the pyrrolopyrrole cyanine intermediate **8** with uncomplexed pyridine and pyrrole units H-PPcy (Schemes S1 and S2 respectively for preparation of reagents **3** and **7**). Following the procedure described by Fischer et al,[19] H-PPcy **8** was obtained by condensation between **3** and **7** with a 68% yield (Scheme 1). The pyrrole and pyridine units of **8** were complexed by boron using either BF_3-OEt_2 (yielding **9**) or $B(Ph)_2Cl$ (yielding **10**) before saponification of the ester groups in mild basic conditions to lead to the desired **TB144** and **TB207** dyes.[20] The electronic absorption spectra of **TB144** and **TB207** are presented in Figure 2a and their spectral properties such as maximal absorption (λ_{abs}), extinction coefficient (ε), wavelength of maximal emission intensity (λ_{em}) and zero-zero energy level of the lowest singlet excited state (E_{00}) are collected in Table 1.

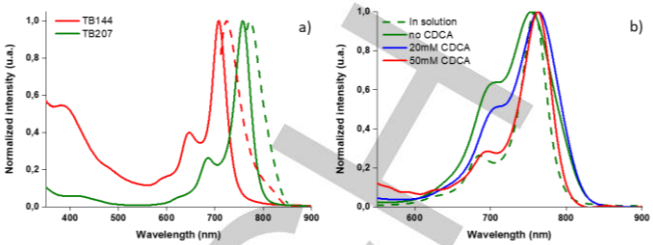

Figure 2. a) Normalized absorption and emission (dashed line) of **TB144** (red line) and **TB207** (black line) recorded in dimethylformamide solution. b) Normalized absorption spectra of **TB207** on 2 μm thick TiO_2 nanocrystalline film 0 mM (black), 20 mM (red) and 50 mM (blue) of CDCA along that in solution (dashed black line).

The absorption spectrum of these new dyes exhibit the classical features of pyrrolopyrrole cyanine derivatives,[21] with a narrow and intense π-π* transition around 750 nm, and a weaker vibronic band at a shorter wavelengths.[22] First, the spectrum of **TB207** is red-shifted relative to that of **TB144** owing to the reduced electron density on boron induced by fluorine, which stabilizes the HOMO level of **TB144** (see DFT calculations below). This result is in agreement with previous reports.[22] Moreover, a bathochromic shift of 28 nm is observed for **TB207** *versus* previously described PPcys derivatives that do not contain anchoring groups.[22] This shift can be attributed to the electron withdrawing effect of carboxylic acid groups that stabilize the LUMO level. Gratifyingly, **TB207** presents almost no absorption in the visible (400-650 nm) and is thus suitable for the development of colourless dye sensitized solar cell with selective NIR-light absorption. On thin TiO_2 film, the intensity of the first absorption band of **TB144** and **TB207**, between 650-720 nm, is increased compared to that in solution witnessing the formation of aggregates (Figure 2b).

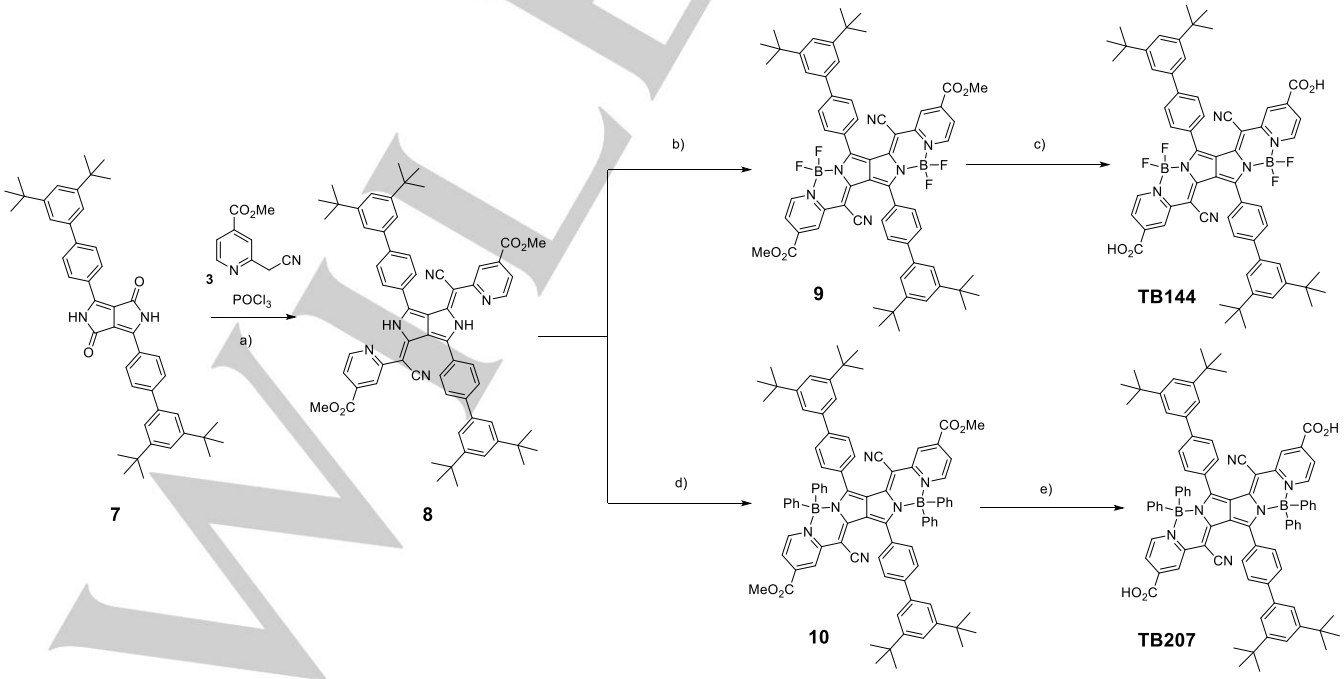

Scheme 1. Synthetic route to pyrrolopyrrole cyanines **TB144** and **TB207**. Reagents and conditions: a) $POCl_3$, 3, Toluene, 130°C, 2 h, 68%; b) BF_3-OEt_2, DIPEA, CH_2Cl_2, 45°C, 30min, 100%; c) LiOH, THF/H_2O, rt, 2h, 72%; d) $B(Ph)_2Cl$, DIPEA, CH_2Cl_2, 45°C, 30min, 41%; e) LiOH, THF/H_2O, rt, 2h, 81%.

However, the addition of chenodeoxycholic acid (CDCA) in the chemisorption bath of **TB207** allows a clear reduction of the aggregate formation and consequently enhances the visible transmittance of the film. Indeed, the green colour due to aggregates fades away (Figure 2b). Comparatively, **TB144** still exhibits aggregation behaviour even when being co-grafted in presence of 50 mM of co-adsorbent agent (Figure S1). Both dyes are quite fluorescent, with rather long lifetimes for low energy lying emitting states, which is a favourable feature in case electron injection is sluggish (Figure 2a and Table 1 and see below transient absorption spectroscopy).

Table 1. Wavelength of maximal absorption (λ_{abs}) with extinction coefficient (ε), wavelength of maximal emission (λ_{em}) recorded at room temperature in dichloromethane and zero-zero energy level of the lowest excited state (E_{00}).

Dye	λ_{abs} /nm (ε/M^{-1}cm^{-1})	λ_{em} /nm	τ_{em} (ns)	E_{00}/eV[a]
TB144	649(20800); 710 (55000)	730	3.7	1,70
TB207	685 (35900); 758(138000)	772	3.2	1.60

[a] calculated with E_{00}= 1240 eV/λ_{inter}, with λ_{inter}= wavelength (in nm) at the intersection of the normalized absorption and emission spectrum

The redox potentials of the dye were investigated by cyclic voltammetry (Figures S2-3) and relevant potentials are given in Table 2. With the zero-to-zero singlet excited state energy level (E_{00}), the electron injection ($\Delta G°_{inj}$) and dye regeneration ($\Delta G°_{reg}$) driving forces can be calculated (Table 2). **TB207** exhibits a reversible one-electron oxidation at 0.82 V *vs.* SCE, corresponding to the formation of the radical cation localized on the pyrrolopyrrole cyanine unit. In contrast, **TB144** presents an irreversible oxidation wave that could be attributed to a lower stability of the radical cation when pyrrolopyrrole cyanine dyes are substituted with fluorine instead of phenyl.[23] The oxidation potential of **TB144** is anodically shifted by about 150 mV relative to that of **TB207** confirming the electron withdrawing character of fluorine on boron in line with DFT calculations (see below). As a result, the Gibbs free energy of electron injection is more exergonic for **TB207** than **TB144**, but logically remains rather modest compared to classical sensitizers with absorption spectrum located in the visible spectrum. To investigate whether **TB207** was chemisorbed on TiO_2 *via* one or two carboxylic groups, attenuated total reflection FT-IR spectra (Figure S4 in SI) were recorded. The dye powder of **TB207** measured as a solid sample shows the intense characteristic stretching band of ν(C=O) at 1728 cm^{-1} of the carboxylic acid groups. After grafting on mesoporous TiO_2 film, the ATR-IR spectrum still displays the presence of the band at 1728 cm^{-1} of free carboxylic acid, *albeit* of lower intensity, along with that of TiO_2 bonded carboxylate at 1650 cm^{-1} and 1385 cm^{-1} corresponding to the asymmetric and symmetric stretching bands respectively. Altogether, these measurements indicate that **TB207** is attached to TiO_2 by only one carboxylic group. This is consistent with the opposite orientation of the two binding groups, which probably prevents them to be both in contact with TiO_2 surface.

Theoretical calculations have been carried out to obtain additional information on the electronic properties of these two dyes (see the SI for details). The two compounds were found to belong to the C_i point group in both their ground and lowest-excited states. Besides indicating that they have null dipole moment in these two states, this symmetry also means that some states are dark. Indeed, as can be seen in Table S1 in the SI, TD-DFT indicates that the lowest excited state, of A_u nature, is strongly allowed and corresponds to the strong absorption band at ca. 700 nm experimentally, whereas the second transition is forbidden (A_g state), which might explain their transparency over a large portion of the visible spectrum. Indeed, in **TB144** the third state, which is dipole allowed, appears at ca. 380 nm consistently with experiment, and the situation is similar in the other compound (Table S1). Theory predicts E_{00} at 1.85 and 1.78 eV, for **TB144** to **TB207**, respectively, reasonably fitting experimental values, the TD-DFT values being slightly blue-shifted, as expected for boron-dyes.[24] The lowest bright transition corresponds to a H-L excitation, and we represent these two orbitals as well as the associated electron density difference plot in Figure 3 for **TB144** (Figure S6 in the SI for **TB207**). The HOMO is localized on the core of the dye, whereas the LUMO is slightly more extended, showing contributions going up to the carboxylic anchoring groups. Nevertheless, the electronic excitation mostly induced changes in the central section of the compound, with rather limited geometrical reorganization, in line with the sharp absorption and emission bands and small Stokes shifts noted experimentally. In going from **TB144** to **TB207** theory predicts that the HOMO is upshifted by 0.29 eV, which is remarkably consistent with the experimental redox potential (0.28 eV, see Table 2) and also fits with the expected relative inductive effects of fluorine atoms and phenyl rings. In the same time, DFT foresees a slightly smaller upshift for the LUMO (+ 0.21 eV), which presents smaller contributions on the nitrogen atoms bonded to the boron centers (in Figure 3), qualitatively explaining the experimental red-shift noticed in going from **TB144** to **TB207**.

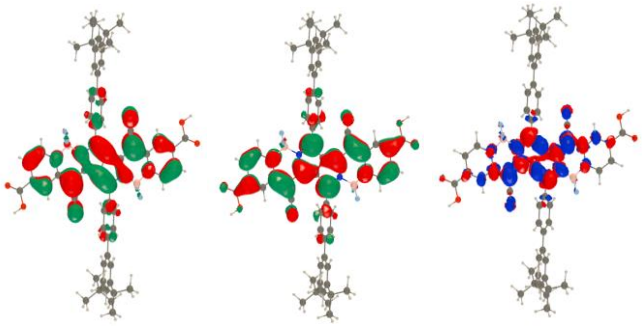

Figure 3. From left to right: HOMO, LUMO and EDD (S_0-S_1) representation for ***TB144***. See Figure S4 in the SI for more details.

Ultrafast Spectroscopy of carrier injection and concurrent processes

As pointed out above (Figure 2b), upon grafting on TiO_2 surfaces, the PPcy sensitizers tend to form aggregates in addition to isolated monomers. Monomer-to-aggregate energy transfer is known to be a main loss channel in kinetic competition with carrier injection from monomers, since it was shown for cyanine and DPP dyes that electrons are rather trapped by low energy states in the aggregates (self-quenching).[14,26,27]

To shed some light on these phenomena, we carried out femtosecond fluorescence and transient absorption experiments of **TB207** grafted on TiO_2 and on Al_2O_3. Due to its higher band gap, Al_2O_3 serves as the reference for a non-injecting electrode.

Table 2. Redox potentials recorded by cyclic voltammetry at room temperature in dimethylformamide solution with Bu_4NPF_6 (0.1M) as supported electrolyte and referenced versus saturated calomel electrode (SCE). Calculated Gibbs free energies for electron injection ($\Delta G°_{inj}$) and dye regeneration ($\Delta G°_{reg}$).

Dye	[a]E(S⁺/S)	[a]E(S/S⁻)	[a]E(S⁺/S*)	[b]ΔG°inj (eV)	[c]ΔG°reg (I3⁻/I⁻) (eV)	[c]ΔG°reg (I⁻,Br⁻)/(I3⁻,I2Br⁻) (eV)	[c]ΔG°reg (disulfide/CH3SO3S⁻) (eV)
TB144	1.10	-	-0.62	-0.08	-0.90	-0.79	-0.60
TB207	0.82	-0.76, -0.51	- 0.80	0.10	-0.62	-0.51	-0.32

[a] determined in V vs. SCE [b] calculated with the equation: $^{a}\Delta G°_{inj}$ = E (S^+/S) – E_{00} + E_{CB} (TiO_2) with $E_{CB}(TiO_2)$ = -0.7 V vs SCE. [c] calculated with the equation : $\Delta G°_{reg}$ = E(M^+/M) - E (S^+/S), with M= redox mediator and E(I_3^-/I^-) = 0.20 V *vs.* SCE, E(I^-,Br^-)/(I_3^-,I_2Br^-) = 0.31 V *vs.* SCE and E(disulfide/$CH_3SO_3S^-$) = 0.39 V *vs.* SCE.

Consequently, energy transfer (ET) is the only excited state quenching process on Al_2O_3 In the following, a complete TiO_2 DSSC with 5 mM CDCA and a 0 mM CDCA Al_2O_3 device were compared since their absorption spectra indicate about the same monomer-to-aggregate ratio (see Figure S5). Figure 4 displays the wavelength-averaged and normalized fluorescence kinetic traces of both devices and of **TB207** in an EtOH/$CHCl_3$ (9/1) solution recorded with 0.2 ps time resolution. The lifetime of **TB207** in solution is 3.2 ns (Table 1 and Figure S7). Both on the TiO_2 and Al_2O_3 DSSC, the excited state of **TB207** is strongly quenched as compared to that in solution and it decays fully in the 1 ns time-window (Figure 4). The fluorescence is dominated by monomer emission, with the excited state quenching being due to monomer-to-aggregate ET for the Al_2O_3 DSSC. On the other hand, the TiO_2 DSSC kinetics decay even faster, because of the additional mechanism of electron injection. A three-exponential fit is required to capture the main decay times. Their values as well as the relative amplitudes are given in Table 3. A simple method of evaluating the carrier injection efficiency is based on the average rates of carrier injection $\langle k_{inj}\rangle$, energy transfer $\langle k_{ET}\rangle$ and monomer excited state decay $\langle k_{mono}\rangle$: $\Phi_{inj} = \langle k\rangle_{inj}/(\langle k\rangle_{inj}+\langle k\rangle_{ET}+\langle k\rangle_{mono})$. Since the former rates largely dominate (Table 3), $\Phi_{inj} \approx \langle k_{inj}\rangle/(\langle k_{inj}\rangle+\langle k_{ET}\rangle)$. With $\langle k\rangle_{Al2O3} = \langle k_{ET}\rangle$ and $\langle k\rangle_{TiO2} = \langle k_{ET}\rangle + \langle k_{inj}\rangle$ we find $\langle k_{ET}\rangle = 0.0185\ ps^{-1}$ and $\langle k_{inj}\rangle = 0.037\ ps^{-1}$, meaning an injection efficiency Φ_{inj} of *ca.* 67 %.

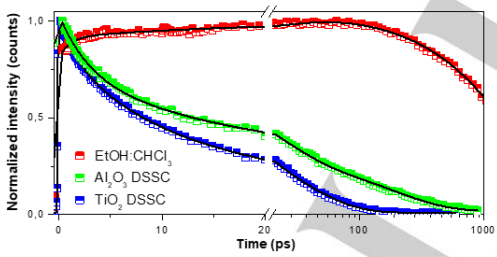

Figure 4. Normalized fluorescence up-conversion kinetic traces, with the respective fitting curves as solid lines, averaged over the fluorescence spectrum of **TB207** in EtOH/$CHCl_3$ (9/1) (red), 0 mM CDCA Al_2O_3 DSSC (green) and 5 mM CDCA TiO_2 DSSC (blue). The samples were excited at 730 nm with 20 μJ/cm². Note the break in the time axis. Log. scale after 20 ps.

Femtosecond TAS reveals the species resulting from the excited state quenching processes, namely the $TB207^+$ cation and excited state absorption of aggregates (Figure S8-S9). It also confirms the time scales found by the fluorescence kinetics, and that, due to structural inhomogeneities both electron injection and ET occur on time scales of roughly 1-100 ps.

The excited state reactions in the **TB207**/TiO_2 DSSC are cast in a reaction scheme illustrated in the ESI (Figure S10). It highlights the kinetic competition between electron injection, where the former wins with a roughly 2/3-to-1/3 excited state branching ratio. Excited aggregates (Agg*) decay on a slower time scale, back to the ground state (S_0), but some contribution to carrier injection and thus to J_{sc} cannot be excluded. [27] In summary, femtosecond fluorescence and TA spectroscopy of **TB207** in a TiO_2 device, prepared with PCE = 3.8% conditions (tri-iodide/iodide electrolyte E1 see below) shows that electron injection outcompetes the ET into residual aggregates. In as much, aggregates may also contribute to the current generation owing to electron injection.

TB207 dye radical cation regeneration and geminate recombination kinetics have been evaluated using a ps pump-probe transient absorption spectroscopy associated with a streak camera for spectral and temporal resolution. The **TB207** radical cation absorbs in the visible region between 530 to 680 nm (Figure S11). The related transient decay corresponds to the dye radical cation depopulation upon a 30 ps pump pulse at 785 nm. It is studied for a I_3^-/I^- based electrolyte (EI) and an inert electrolyte (E1 without redox mediator). The exponential decay required two components. For I_3^-/I^- redox couple, the regeneration takes place within τ_1= 0.38 μs (±0.02 μs) (f_1 = 72 %) and τ_2= 2.52 μs (±0.16 μs) (f_2 = 28 %) (Figures S11a, S12a). These values are almost one order of magnitude faster than those reported for conventional dyes such as D-π-A dyes or ruthenium complexes.[26–28] As confirmed by the fs-TAS and upconversion studies, aggregates contribute to the carrier injection. As such, it is convenient to assign the faster component to the regeneration of the dye monomer while the slower one is attributed to the dye aggregate regeneration. Moreover, the lifetime of **TB207** radical cation with a redox-free inert electrolyte shows long-lived species within τ_1= 85.3 μs (± 8.3 μs) and τ_2= 868.5 μs (± 51.6 μs) (Figures S11b, S12b). A simple method of evaluating the dye regeneration efficiency Φ_{reg} is based on the average rates of dye radical cation regeneration $\langle k_{reg}\rangle$, and geminate recombination decay $\langle k_{rec}\rangle$: $\Phi_{reg} = \langle k_{reg}\rangle / (\langle k_{reg}\rangle + \langle k_{rec}\rangle)$. The measured kinetics reveals a $\langle k_{reg}\rangle = 1.031\ \mu s^{-1}$ and $\langle k_{rec}\rangle = 2.78\ 10^{-3}\ \mu s^{-1}$, which means a dye regeneration efficiency Φ_{reg} = 99.7 %. Even though the geminate recombination kinetics of **TB207** is faster than for **VG20** cyanine dye counterpart (0.94 ms ± 0.02 ms),[13] it remains slow enough compared to the two orders of magnitude faster regeneration, thus allowing devices to reach quantitative regeneration yields with this new family of dyes.

Photovoltaics characterization

With the encouraging results of the above photophysical study, the photovoltaic performances of **TB144** and **TB207** dyes were then investigated in DSSCs. They were first studied with the conventional electrolyte based on I_3^-/I^- redox mediator. The optimal electrolyte composition requires to get rid of the typical

Table 3. Time constants obtained by fitting the kinetic traces of Figure 7 with a sum of 3 exponentials convoluted with a 150-fs Gaussian (temporal resolution). <τ> and <k> refer to the average lifetime and the corresponding average rate.

Sample	A1%	τ1/ps	A2%	τ2/ps	A3%	τ3/ps	<τ>/ps
Al_2O_3 DSSC	35	2.0	39	17	26	180	54.1
TiO_2 DSSC	16	1.5	43	8	41	35	18.0

additives of 4-tert-butylpyridine (4-TBP) and the guanidinium thiocyanate (GuSCN) as they shift the TiO_2 conduction band edge to a more negative potential and would therefore importantly compromise electron injection efficiency.[29,30] The electrolyte (coded **EI**) also includes a high concentration of Li^+ (1 mol/L), because small alkali cations are known for their specific absorption properties upon the surface of TiO_2. This results in the downshift of the flat band potential and the trap states energy accordingly to Nernst equation (59 mV down by one decade of the alkali cation concentration), thus guaranteeing enough driving force for the charge injection. These conditions are rather usual with NIR sensitizers.[13] As aforesaid, the pyrrolopyrrole cyanine dyes tend to aggregate, and this can severely decrease the performances of the NIR-DSSC. Accordingly, the solar cells were fabricated with CDCA during chemisorption of dye to limit the self-quenching by ET on TiO_2.[31–33] Increasing the CDCA amount into the dye bath decreases the film's coloration, which is ascribed to the reduction of both the dye loading and molecular aggregations. Even though CDCA acts as a co-adsorbent in this range of concentration,[34] the underlying loss of dye loading and thus NIR light capture by the photo-anode is highly counterbalanced by the better charge separation and injection processes.

As shown in Figure S1, **TB144** still exhibits strong presence of aggregation even after adding 50 mM of CDCA in the chemisorption bath. The 1/500 ratio leads to a maximum PCE of 1.2% for **TB144** dye (J_{sc}= 5.18 mA/cm², V_{OC}= 333 mV and FF= 62%) as shown in the J-V curve of Figure 5.

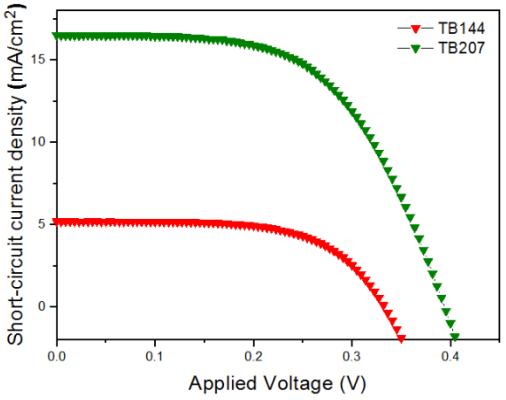

Figure 5. J-V curves of **TB144** dye with 50 mmol/L of CDCA in the sensitizing solution (red) and **TB207** with 5 mmol/L of CDCA (green). The electrolyte composition was 1 mol/L DMII, 1 mol/L LiTFSI, and 0.03 mol/L I_2 in acetonitrile/valeronitrile (85/15 v/v) solvent mixture.

For **TB207** dye, a remarkable performance has been achieved even without CDCA, as 3.2 % PCE was recorded. The increment of CDCA concentration to 5 mmol/L in the **TB207** dye solution allows achieving a PCE maximum of 3.9% (Figure 5), owing to an increase in J_{SC} from 15.7 to 16.5 mA/cm², and a *ca.* 50 mV enhancement in the open-circuit voltage (V_{oc}) from 348 mV to 394 mV. A further increase in the CDCA concentration up to 10 mmol/L (corresponding to 1/100 ratio) leads to a slight drop in J_{sc} to 14.9 mA/cm² leading to a final PCE of 3.4 % (Figure S13). The J_{SC} drop with 10 mmol/L of CDCA can be attributed to the competition between the dyes and CDCA molecules adsorbed on the TiO_2 surface. As such, the optimized condition for **TB207** is a 1/50 ratio by concentration between the dye and CDCA. The characteristics of all the solar cells are gathered in Table S2.

Deciphering the limitations of reaching higher PCE values, the open-circuit voltage (V_{oc}) appears to be one main contributor controlling final PCE. Moreover, the non-geminate recombination of the electrons in the TiO_2 to the oxidized species in the electrolyte (*e.g.*, I_3^-) is also considered at the origin affecting V_{oc}, resulting systematically in lower PCE. An interhalogen based binary-redox couple was proposed by Lee et al., denoted by (I_3^-, I_2Br^-)/(I^-,Br^-). This binary redox couple has a stronger oxidant strength than the classical I_3^-/I^-, which would be favorable to reduce internal energy losses related to the dye regeneration.[35] As a result, integrating this interhalogen binary-electrolyte (coded **B1**) with NIR PPcy dye **TB207** increases the V_{oc} by more than 30 mV, reaching 430 mV (Figure 6a). Despite the slight drop in the J_{sc}, and with a ff = 0.59, this voltage gain affords to reach a 4.0% PCE, a never reached value for NIR-selective DSSC.

Intensity-modulated photovoltage/photocurrent spectroscopy (IMVS/PS) experiments (Figure 6b-c) show that the introduction of binary redox system with bromide affects mainly the electron lifetime, compared to EI. This implies that the interhalogen species in the binary electrolyte reduce the non-geminate recombination by *ca.* two times, helping increase V_{oc}, in agreement with the previous studies in the literature.[35,36]

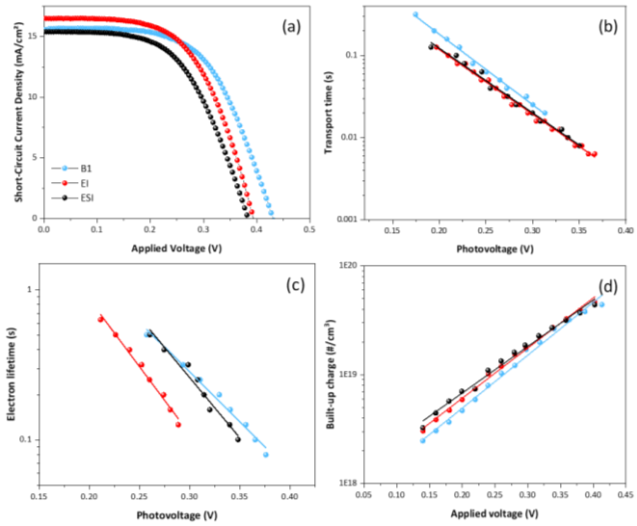

Figure 6. (a) J-V curve evolution of **TB207**-based DSSC with different electrolytes: B (I_3^-,I_2Br^-)/ (I^-,Br^-) in blue, EI I_3^-/I^- in red, and ESI in black. (b) IMPS, (c) IMVS, and (d) dark charge extraction measurements on **TB207**-DSSC are presented with the different electrolytes.

The transport time was affected to a less extent, which leads to charge collection efficiency of 92 and 81 % for (I_3^-,I_2Br^-)/ (I^-,Br^-)

and I_3^-/I^--based devices, respectively. The additional dark charge extraction experiment suggests that the trap energies are not drastically affected by the different electrolytes, which implies almost no change in the surface states below the conduction band of TiO_2 nanoparticles upon the variation of the redox species in the electrolyte, which is in agreement to literature (Figure 6d).
Even though replacing I_3^-/I^- with the interhalogen binary redox couple (I_3^-,I_2Br^-)/ (I^-,Br^-) increases the PCE, the aesthetics are not enhanced as both electrolytes exhibit a fingerprint in the blue range of the visible spectrum (293 and 362 nm) as shown in Figure S14, leading to the final similar yellowish coloration. These bands correspond to the light absorption by the tri-iodide species. Cong et al. introduced back in 2012 a transparent and colorless sulfur/iodide-based hybrid electrolyte that enhanced the performance of the benchmark Ru complex dye N719.[37] This concept of hybrid electrolyte was recently introduced for the NIR-cyanine dye VG20 using a methyl sulfite thiolate ($CH_3SO_3S^-$) with iodide (coded **ESI**) leading to as high as 80% AVT and CRI 96. **ESI** electrolyte shows negligible absorption in the visible region (Figure S14) and thus was introduced with **TB207** dye. When the TiO_2 film is sheltered with a scattering layer, a maximum PCE of 3.3% is achieved (Figure 6a) (J_{sc}= 15.40 mA/cm², V_{oc}= 384 mV, and ff = 0.55). IMVS and IMPS results, presented in Figure 6b-c, indicate no drastic modification in electron lifetime and transport time by substituting EI electrolyte with ESI electrolyte. As the scattering TiO_2 is removed to achieve transparent devices, the J_{sc} reaches 10.9 mA/cm², while V_{oc} increases to 408 mV and ff to 0.56, leading to a 2.5% PCE for a fully transparent **TB207**-based DSSC (Figure S15). The performance of the transparent **TB207**-DSSC with EI electrolyte is similar to ESI one (J_{sc}= 11.8 mA/cm², V_{oc}= 376 mV, and FF= 0.57, PCE = 2.5%). This new family of dye shows improved stability compared to the state-of-the art NIR-selective VG20-C_{16} dye, retaining 80% of initial PCE after 300 hours shelf-life (Figure S16).

TB207 devices based on 4 µm-TiO_2 and EI electrolyte reaches an excellent AVT of 75%, leading to a light utilization efficiency (LUE) of 1.8%, which is an excellent value given the TPV applications.[1] As presented in Figure 7a, these devices are positioned at x= 0.3686, y= 0.4045 in the CIE 1931 chromaticity diagram with a CRI of 90 (CCT= 4565 K). The dominant wavelength is determined to be at 570 nm, a wavelength representing an orange-yellow color. The color purity of the perceived light through the **TB207**-based devices with EI electrolyte is 0.32. It is important to understand that as the color purity is close to zero, it is near the reference white point and represents a very pale color.[38] The advantage of the hybrid thiolate/iodide electrolyte (ESI) lies in its negligible absorbance in the whole visible region (Figure 7b), allowing the **TB207**-based devices to reach a high AVT value of 76% with an excellent CRI of 93. The x,y 1931 CIE chromaticity coordinates move closer to the position of the white reference point (Figure 7.a) as we replace the triiodide/iodide or the binary interhalogen electrolyte with the thiolate/iodide hybrid one (x= 0.3474, y= 0.3703, CCT= 5125 K). The determined dominant wavelength is 570 nm with a color purity of 0.16. This indicates that even the dominant color perceived is greenish-yellow due to the residual weak dye absorption, the very low color purity makes it appear highly color neutral.

In conclusion, this study highlights, for the first time, the real potential of pyrrolopyrrole cyanine as sensitizers for selective NIR-DSSC and particularly for the development of TPV. On one hand, the replacement of fluoride by a phenyl group on boron importantly increases the photovoltaic performances of the dye by enhancing electron injection driving force and reducing the formation of aggregates. On the other hand, this new class of dye is particularly promising because a simple system such as **TB207** already gives the highest power conversion efficiency ever reported for transparent and colorless DSSC and with a very high AVT and CRI values. It is thus reasonable to assume that the numerous possibilities of functionalization of pyrrolopyrrole cyanine will enable to reach higher performances and higher aesthetic features upon new molecular designs of this class of dyes. Moreover, pyrrolopyrrole cyanine dyes could be most certainly implemented with sensitizers absorbing in the visible spectrum to develop panchromatic cocktail dyes or tandem solar cells and for dye sensitized photocatalytic systems to exploit low energy photons.

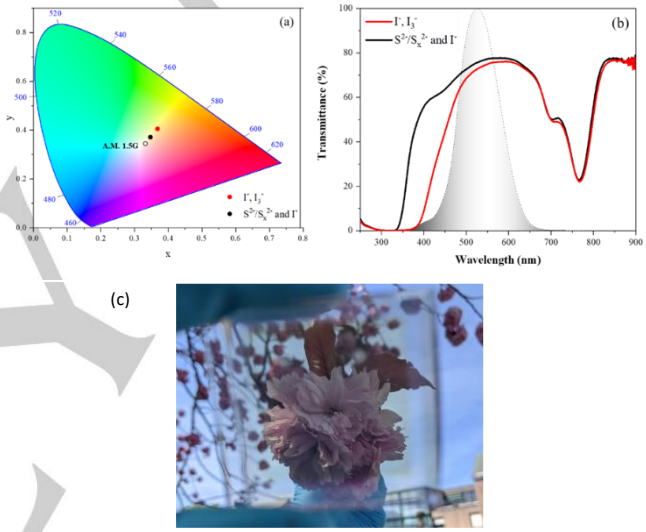

Figure 7. (a) CIE 1931 chromaticity diagram showing the positions of the **TB207**-based DSSC with I^-/I_3^- electrolyte (red) and the hybrid thiolate/iodide electrolyte (black). The white point represents our illumination source used in the study AM 1.5G. (b) Transmittance spectra of a 4 µm-TiO_2-based DSSC with **TB207** dye and I^-/I_3^- electrolyte (red) and the hybrid thiolate/I^- electrolyte (black). The shaded grey area represents the human's eye photopic response. (c) a typical picture of the TB207-based DSSC including ESI electrolyte.

Experimental Section

All Experimental Procedures/Data are in the Supporting Information. Further UV−visible absorption spectroscopy experiments in solution and on mesoscopic TiO_2 film, distribution of the molecular frontier orbitals, cyclic voltamperometry, photoluminescence and TA decays in solution or devices, additional J−V curves under illumination, ^{1}H NMR spectra mass spectra of the new compounds.

Acknowledgements

We acknowledge financial support by Agence National de la Recherche (ANR) through the program Vision-NIR (ANR-17-CE05-0037-02) and ANR for the EUR project LUMOMAT. S.F. acknowledges the “IMPRESSIVE” project which received funding from the European Union’s Horizon2020 research and innovation program under grant agreement number no. 826013. D.J.

acknowledges the CCIPL/Glicid computational center installed in Nantes for the generous allocation of computational resources. The authors greatly acknowledge J. Hémez and L. Arzel (AMaCC platform, CEISAM UMR CNRS 6230, University of Nantes) for the mass spectrometry analyses.

Keywords: Photovoltaics, Transparency, DSSC, NIR, Pyrrolopyrrole cyanine

[1] C. J. Traverse, R. Pandey, M. C. Barr, R. R. Lunt, *Nature Energy* **2017**, *2*, 849–860.

[2] G. P. Kini, S. J. Jeon, D. K. Moon, *Adv. Funct. Mater***. 2021**, *31*, 2007931.

[3] E. Ravishankar, M. Charles, Y. Xiong, R. Henry, J. Swift, J. Rech, J. Calero, S. Cho, R. E. Booth, T. Kim, A. H. Balzer, Y. Qin, C. Hoi Yi Ho, F. So, N. Stingelin, A. Amassian, C. Saravitz, W. You, H. Ade, H. Sederoff, B. T. O'Connor, *Cell Reports Phys. Sci.* **2021**, *2*, 100381.

[4] K. Lee, H.-D. Um, D. Choi, J. Park, N. Kim, H. Kim, K. Seo, *Cell Reports Phys. Sci.* **2020**, *1*, 100143.

[5] C. Yang, D. Liu, M. Bates, M. C. Barr, R. R. Lunt, *Joule* **2019**, *3*, 1803–1809.

[6] A. Hagfeldt, G. Boschloo, L. Sun, L. Kloo, H. Pettersson, *Chem. Rev.* **2010**, *110*, 6595–6663.

[7] M. K. Nazeeruddin, P. Péchy, M. Grätzel, *Chem. Commun.* **1997**, *0*, 1705–1706.

[8] T. Kinoshita, K. Nonomura, N. Joong Jeon, F. Giordano, A. Abate, S. Uchida, T. Kubo, S. I. Seok, M. K. Nazeeruddin, A. Hagfeldt, M. Grätzel, H. Segawa, *Nat Commun* **2015**, *6*, 8834.

[9] T. Swetha, K. R. Reddy, S. P. Singh, *Chem. Record* **2015**, *15*, 457–474.

[10] Y. Hao, X. Yang, J. Cong, H. Tian, A. Hagfeldt, L. Sun, *Chem. Commun.* **2009**, 4031–4033.

[11] N. P. Liyanage, A. Yella, M. Nazeeruddin, M. Grätzel, J. H. Delcamp, *ACS Appl. Mater. Interfaces* **2016**, *8*, 5376–5384.

[12] K. Zhang, C. Qin, X. Yang, A. Islam, S. Zhang, H. Chen, L. Han, *Adv. Energy Mater.* **2014**, *4*, 1301966.

[13] W. Naim, V. Novelli, I. Nikolinakos, N. Barbero, I. Dzeba, F. Grifoni, Y. Ren, T. Alnasser, A. Velardo, R. Borrelli, S. Haacke, S. M. Zakeeruddin, M. Graetzel, C. Barolo, F. Sauvage, *JACS Au* **2021**, *1*, 409–426.

[14] A. Mishra, M. K. R. Fischer, P. Bäuerle, *Angew. Chem. Int. Ed.* **2009**, *48*, 2474–2499.

[15] S. Huang, C. Yang, J. Huang, X. Wang, M. Wang, *Dyes Pigments* **2018**, *154*, 269–274.

[16] C. Yang, X. Wang, M. Wang, K. Xu, C. Xu, *Chem. – A Eur. J.* **2017**, *23*, 4310–4319.

[17] S. Huang, W. Liu, J. Huang, X. Wang, C. Yang, H. Bohra, Q. Liu, M. Wang, *ACS Appl. Bio Mater.* **2018**, *1*, 1109–1117.

[18] M. Bai, S. Achilefu, *Heterocycl. Commun*. **2010**, *16*, 213–216.

[19] G. M. Fischer, M. K. Klein, E. Daltrozzo, A. Zumbusch, *Eur. J. Org. Chem.* **2011**, *2011*, 3421–3429.

[20] D. Kumaresan, R. P. Thummel, T. Bura, G. Ulrich, R. Ziessel, *Chem. – A Eur. J.* **2009**, *15*, 6335–6339.

[21] G. M. Fischer, E. Daltrozzo, A. Zumbusch, *Angew. Chem. Inter. Ed.* **2011**, *50*, 1406–1409.

[22] G. M. Fischer, M. Isomäki-Krondahl, I. Göttker-Schnetmann, E. Daltrozzo, A. Zumbusch, *Chem. – A Eur. J.* **2009**, *15*, 4857–4864.

[23] E. M. Espinoza, J. A. Clark, J. Soliman, J. B. Derr, M. Morales, V. I. Vullev, *J. Electrochem. Soc.* **2019**, *166*, H3175.

[24] B. Le Guennic, D. Jacquemin, *Acc. Chem. Res.* **2015**, *48*, 530–537.

[25] M. Kawasaki, S. Aoyama, *Chem. Commun.* **2004**, 988–989.

[26] F. Sauvage, S. Chhor, A. Marchioro, J.-E. Moser, M. Graetzel, *J. Am. Chem. Soc.* **2011**, *133*, 13103–13109.

[27] A. Y. Anderson, P. R. F. Barnes, J. R. Durrant, B. C. O'Regan, *J. Phys. Chem. C* **2011**, *115*, 2439–2447.

[28] M. Ansari-Rad, *J. Phys. Chem. C* **2016**, *120*, 9000–9006.

[29] S. E. Koops, B. C. O'Regan, P. R. F. Barnes, J. R. Durrant, *J. Am. Chem. Soc.* **2009**, *131*, 4808–4818.

[30] G. Boschloo, L. Häggman, A. Hagfeldt, *J. Phys. Chem. B* **2006**, *110*, 13144–13150.

[31] A. Kay, M. Graetzel, *J. Phys. Chem.* **1993**, *97*, 6272–6277.

[32] J. A. Anta, E. Guillén, R. Tena-Zaera, *J. Phys. Chem. C* **2012**, *116*, 11413–11425.

[33] L. Zhang, J. M. Cole, *J. Mater. Chem. A* **2017**, *5*, 19541–19559.

[34] A. K. Chandiran, S. M. Zakeeruddin, R. Humphry-Baker, M. K. Nazeeruddin, M. Grätzel, F. Sauvage, *ChemPhysChem* **2017**, *18*, 2724–2731.

[35] N. C. D. Nath, H. J. Lee, W.-Y. Choi, J.-J. Lee, *Electrochim. Acta* **2013**, *109*, 39–45.

[36] N. C. D. Nath, J.-J. Lee, *J. Ind. Eng. Chem.* **2019**, *78*, 53–65.

[37] J. Cong, X. Yang, Y. Hao, L. Kloo, L. Sun, *RSC Adv.* **2012**, *2*, 3625–3629.

[38] E. F. Schubert, *Light-Emitting Diodes*, Cambridge University Press, Cambridge, **2006**.